AJNR Am J Neuroradiol 25:997–1005, June/July 2004

Dynamic Susceptibility Contrast-Enhanced Perfusion and Conventional MR Imaging Findings for Adult Patients with Cerebral Primitive Neuroectodermal Tumors

Meng Law, Khuram Kazmi, Stephan Wetzel, Edwin Wang, Codrin Iacob, David Zagzag, John G. Golfinos, and Glyn Johnson

BACKGROUND AND PURPOSE: **Preoperative differentiation of primitive neuroectodermal tumors (PNETs) from other tumors is important for presurgical staging, intraoperative management, and postoperative treatment. Dynamic, susceptibility-weighted, contrast-enhanced MR imaging can provide in vivo assessment of the microvasculature in intracranial mass lesions. The purpose of this study was to determine the perfusion characteristics of adult cerebral PNETs and to compare those values with low and high grade gliomas.**

METHODS: **Conventional MR images of 12 adult patients with pathologically proved cerebral PNETs were analyzed and provided a preoperative diagnosis. Relative cerebral blood volume (rCBV) measurements and estimates of the vascular permeability transfer constant, K^{trans}, derived by a pharmacokinetic modeling algorithm, were also obtained. These results were compared with rCBV and K^{trans} values obtained in a group of low grade gliomas (n = 30) and a group of high grade gliomas (n = 55) by using a Student *t* test.**

RESULTS: **On conventional MR images, PNETs were generally well-defined contrast-enhancing masses with solid and cystic components, little or no surrounding edema, and occasional regions of susceptibility. The rCBV of cerebral PNETs was 4.76 ± 1.99 SD, and the K^{trans} was 0.0033 ± 0.0035. A comparative group of patients with low grade gliomas (n = 30) had significantly lower rCBV ($P < .0005$) and lower K^{trans} ($P < .05$). Comparison with a group of high grade gliomas showed no statistical significance in the rCBV and K^{trans} ($P = .53$ and .19, respectively).**

CONCLUSION: **Dynamic, susceptibility-weighted, contrast-enhanced MR imaging shows areas of increased cerebral blood volume and vascular permeability in PNETs. These results may be helpful in the diagnosis and preoperative differentiation between PNETs and other intracranial mass lesions (such as low grade gliomas), which have decreased perfusion but may sometimes have a similar conventional MR imaging appearance.**

Primitive neuroectodermal tumors (PNETs) are classified as embryonal tumors. PNETs can be further subclassified according to location as cerebral PNETs and medulloblastomas. Cerebral PNETs are very rare tumors and account for <5% of all intracranial tumors in children (1). Only a small number of PNETs have been described as occurring in adults (2–5), with one report describing the neuroradiologic findings of PNETs in five adult patients (6).

The preoperative diagnosis of PNET and the determination of tumor vascularity has potential surgical and clinical implications: 1) accurate clinical staging requires spinal MR imaging to exclude spinal metastases; 2) the sensitivity of these tumors to chemotherapy and radiation therapy makes adjuvant therapy a very important option, with or without surgery; 3) in patients with hydrocephalus, the placement of a ventriculoperitoneal shunt should be considered only if absolutely necessary because of the risk of CSF

Received August 12, 2003; accepted after revision October 31.

Supported by Grant RO1CA093992 from the National Cancer Institute/National Institutes of Health.

Presented at the annual meeting of the American Society of Neuroradiology, Washington, DC, April 2003.

From the Departments of Radiology (M.L., K.K., S.W., E.W., G.J.), Pathology (C.I., D.Z.), and Neurosurgery (J.G.G.), New York University Medical Center, New York, NY.

Address reprint requests to Meng Law, MD, Department of Radiology, New York University Medical Center, Magnetic Resonance Imaging Department, Schwartz Building, Basement HCC, 530 First Avenue, New York, NY 10016.

© American Society of Neuroradiology

TABLE 1: Conventional MR imaging findings in primitive neuroectodermal tumors

Patient No.	Volume (cm^3)	T1 Signal	T2 Signal	Enhancement* (%)	Edema	Mass Effect	Necrotic/ Cystic	Lesion Delineation	Heterogeneity	Calcification
1	5 × 3 × 2.5	Iso	Iso	50	+	+	Yes	Well	Yes	Yes
2	2.5 × 2 × 2	Iso	Hypo	90	−	+	Yes	Well	Yes	No
3	6 × 6 × 6	Hypo	Iso	30	++	+++	Yes	Well	Yes	No
4	6 × 6 × 6	Hypo	Iso	80	+	++	Yes	Well	Yes	No
5	3.5 × 2.5 × 1.5	Iso	Hyper	70	++	+	Yes	Well	Yes	No
6	3.5 × 4 × 3	Hypo	Hyper	50	+	++	Yes	Ill	Yes	Yes
7	5 × 3 × 2	Iso	Iso	50	+	+	Yes	Ill	Yes	No
8	2.5 × 1.5 × 2	Iso	Hyper	80	−	−	No	Well	No	No
9	3 × 3 × 3	Iso	Hyper	90	+	+	No	Well	Yes	No
10	7 × 6 × 5	Iso	Iso	30	++	+++	Yes	Well	Yes	Yes
11	1.5 × 2 × 2	Iso	Hypo	50	+++	+	Yes	Well	Yes	No
12	1 × 1 × 1	Iso	Hypo	50	−	−	No	Well	No	No

Note.—Iso indicates isointense to gray matter; Hypo, hypointense; Hyper, hyperintense; +, mild; ++, moderate; +++, severe.

* Enhancement is shown as the percentage of the lesion volume that enhanced.

spread and seeding (7, 8); 4) in more eloquent parts of the supratentorial brain, and obviously in the brain stem where the neurosurgeon may be hesitant to perform a biopsy, particularly when the differential diagnosis may include a low grade glioma and a PNET, characterizing the vascularity of a lesion, and hence its aggressiveness, may assist the neurosurgeon in making a decision regarding biopsy; 5) finally, a neurosurgeon confronted with a contrast-enhancing, highly cellular tumor shown by preoperative MR imaging often will rely on intraoperative frozen section diagnosis to decide between limited biopsy and aggressive resection. Preoperative suspicion of PNET based on dynamic, susceptibility-weighted, contrast-enhanced MR imaging (DSC MR imaging) may allow the neurosurgeon to proceed aggressively. More importantly, it may bolster the surgeon's faith in the intraoperative pathologic diagnosis of PNET.

DSC MR imaging is proving to be a valuable tool in the assessment of intracranial mass lesions. It provides physiological information regarding tumor microcirculation and hemodynamics that is not provided by conventional MR imaging (9–14). More recently, investigators have also shown the usefulness of vascular permeability measurements in the characterization of tumor hemodynamics (15–17). Numerous animal experiments have been conducted to investigate new tracers and techniques for measuring blood volume and vascular permeability simultaneously (18–20). Ultra high field, high resolution MR imaging at 8 T and above can also allow visualization of microvascularity in normal and diseased brain (21, 22).

The purpose of this study was to further elucidate the MR imaging appearance of these rare tumors and to investigate whether relative cerebral blood volume (rCBV) and vascular permeability (K^{trans}) measurements would help in differentiating these tumors from other brain neoplasms. We hypothesized that because PNETs are highly aggressive tumors, rCBV and K^{trans} would be elevated and would allow differentiation between PNETs and low grade but not high grade gliomas.

Methods

Patients and Histopathologic Analysis

All patients referred for stereotactic biopsy or stereotactic volumetric resection of brain tumors at our institution between January 1, 1996, and June 1, 2003, were included in this study. A retrospective analysis of our database of 2754 patients who had undergone DSC MR imaging in addition to conventional MR imaging revealed 12 adult patients with histologically proved cerebral PNETs (Table 1). At our institution, DSC MR imaging is performed simultaneously with conventional MR imaging as part of the routine workup for tumors. Histopathologic specimens were reviewed by two board-certified neuropathologists (C.I., D.Z.) who classified the tumors as cerebral PNETs according to the World Health Organization classification (23). Two board-certified neuropathologists were involved in performing a case-by-case correlation between the DSC MR imaging findings and histopathologic findings. Patients included eight men and four women, ranging in age from 22 to 83 years (mean age, 46.5 years) (Table 2). The low grade glioma group (n = 30) was comprised of 20 low grade gliomas and 10 low grade oligodendrogliomas. Pilocytic astrocytomas were not included in this study because even though they are classified as a World Health Organization grade 1 neoplasm, the nodule of enhancement often seen with these tumors indicates elevated rCBV and permeability, putting these tumors into a different group of lesions in terms of perfusion characteristics. The high grade glioma lesions (n = 55) were all either anaplastic astrocytomas (n = 16) or glioblastoma multiforme (n = 39). Approval for this study was obtained from our institutional review board.

Conventional MR Imaging and Perfusion Data Acquisition

MR imaging was performed with the use of 1.5-T systems. A localizing sagittal view T1-weighted image and then unenhanced axial view T1-weighted (600/14/1 [TR/TE/NEX]) and T2-weighted (3400/119/1) images were obtained. Contrast-enhanced axial view (600/14) T1-weighted images were obtained after the perfusion data were acquired. Conventional MR imaging findings were reviewed by a board-certified neuroradiologist (E.W.) for tumor size, tumor location, signal intensity characteristics, contrast enhancement, presence of calcification/hemorrhage, and presence of cystic/necrotic components. For tumor size, the three orthogonal maximal diameters were measured (Table 1). Tumor volume was calculated by using the ellipsoid formula $\pi/6 \times$ the three orthogonal maximal diameters of the lesion. Lesion signal intensity characteristics were classified as hypo-, iso-, or hyperintense relative to gray matter

TABLE 2: Relative cerebral blood volume measurements and vascular permeability measurements in patients with primitive neuroectodermal tumors

Patient No.	Age (y)/Sex	Location	rCBV	SD	K^{trans}	SD
1	28/M	Temp/brain stem/cerebellum	8.90		3.00×10^{-04}	
2	37/F	Thalamus/brain stem	3.33		5.70×10^{-03}	
3	42/M	Right frontal	4.28		9.20×10^{-03}	
4	68/M	Bifrontal	3.97		1.20×10^{-03}	
5	58/M	Right frontal	6.98		1.70×10^{-04}	
6	52/M	Right frontal	4.34		4.80×10^{-05}	
7	46/M	Right temporal	5.43		8.40×10^{-03}	
8	46/F	Pineal	5.11		5.20×10^{-03}	
9	83/F	Left parietal	2.72		5.90×10^{-04}	
10	42/M	Temporoparietal	2.28		3.35×10^{-05}	
11	34/F	Bifrontal	6.82		3.40×10^{-04}	
12	22/M	Suprasellar	2.91		2.00×10^{-03}	
Mean	46.50		4.76	1.99	0.0033	0.0035

Note.—M indicates male; F, female; Temp, temporal; rCBV, relative cerebral blood volume; K^{trans}, vascular permeability (s^{-1}).

on T1- and T2-weighted images. The extent of contrast enhancement was estimated as a percentage of the total lesion volume. The amount of edema and mass effect was graded as mild (+), moderate (++), or severe (+++).

DSC MR Imaging Data Acquisition

DSC MR images were acquired with a gradient-echo echo-planar imaging sequence during the first pass of a standard dose (0.1 mmol/kg) bolus of gadopentetate dimeglumine (Magnevist; Berlex Laboratories, Wayne, NY). Seven to 10 sections were selected through the tumor on the basis of T2-weighted and fluid-attenuated inversion recovery findings. Imaging parameters were as follows: field of view, 230 × 230 mm; section thickness, 5 mm; matrix, 128 × 128; in-plane voxel size, 1.8 × 1.8 mm; intersection gap, 0 to 2 mm; flip angle, 30 degrees; signal intensity bandwidth, 1470 Hz/pixel. A series of 60 multisection sets were acquired at one-second intervals. Contrast medium was injected at the 10th acquisition at a rate of 5 mL/s, and then a 20-mL bolus of saline was administered at a rate of 5 mL/s.

Perfusion Data Postprocessing rCBV

Standard algorithms were used to calculate rCBV from the DSC MR imaging data (11, 24). Data processing was performed on a Unix workstation with programs developed in-house by using C and IDL programming languages. Cerebral blood volume was measured in regions of interest positioned within the tumor and expressed relative to measurements made in a region of interest in contralateral white matter. To minimize confounding factors in rCBV analysis, the size of the regions of interest was kept constant (radius = 3.6 mm). Regions of interest were positioned in areas of maximal abnormality based on color maps. This approach has been shown to provide the highest intra- and interobserver reproducibility (25). Measurements were obtained by a neuroradiologist (M.L. or S.W.) experienced in perfusion data acquisition at our institution.

First Pass Pharmacokinetic Modeling for Vascular Permeability

First pass pharmacokinetic modeling (26) was used to calculate K^{trans} from the same DSC MR imaging data used to calculate rCBV. First pass pharmacokinetic modeling uses an exact expression for tissue contrast concentration, assuming that contrast medium exists in two interchanging compartments (plasma and extravascular, extracellular space). An estimate of vascular contrast medium concentration is acquired from normal white matter and fitted to the tissue concentration expression to derive K^{trans}. K^{trans} was measured in regions of interest showing the highest permeability based on a map of signal intensity drop 25 seconds after the bolus peak (SD25 color overlay map). K^{trans} measurements were obtained by a neuroradiologist (M.L. or S.W.) experienced in perfusion data acquisition at our institution.

The following derivation for K^{trans} is similar to one reported by Tofts and Kermode (27); it includes the internationally agreed upon standardized nomenclature presented by Tofts et al (28). Flow of tracer into the extravascular extracellular space is described by the following equation:

$$1) \qquad v_e \frac{dC_e}{dt} = K^{trans}(C_p - C_e)$$

where v_e is the fractional extravascular extracellular space volume, C_e and C_p are the tracer concentrations in the extravascular extracellular space and plasma, respectively, and K^{trans} is the transfer constant.

The solution of the first order differential equation (equation 1) is as follows:

$$2) \qquad C_e = \frac{K^{trans}}{v_e}\int_0^t C_p(t')\exp\left(-\frac{K^{trans}}{v_e}(t-t')\right)dt'.$$

Total tissue concentration, C_t, is then as follows:

$$3) \quad C_t = v_pC_p + v_eC_e = v_pC_p + K^{trans}\int_0^t C_p(t')\exp\left(-\frac{K^{trans}}{v_e}(t-t')\right)dt'$$

where v_p is the fractional plasma volume.

An estimate of C_p is acquired from a region of normal white matter, assuming a literature value of plasma volume in the normal white matter. This estimate of C_p can then be fitted to the model function, equation 3, with K^{trans}, v_e, and v_p as fitting parameters.

Statistical Analysis

A Student *t* test was conducted to compare perfusion parameters of PNETs and low and high grade gliomas.

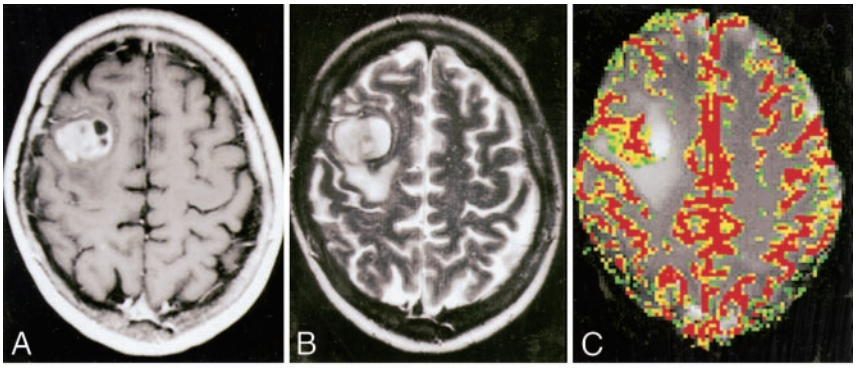

FIG 1. Images of a 58-year-old man (patient 5) with resection-proved PNET.

A, Contrast-enhanced axial view T1-weighted image (600/14/1) shows a fairly well-defined enhancing mass in the right frontal region. Approximately 70% of the lesion enhanced. Cystic/necrotic components can be seen in the lesion.

B, Axial view T2-weighted image (3400/119/1) shows some areas of hypointensity within the mass, with a small amount of peritumoral edema and mass effect.

C, Gradient-echo axial view perfusion MR image (1000/54) and rCBV color overlay map show increased perfusion with a high rCBV of 6.98 and vascular permeability (K^{trans}) of 0.00017 s^{-1}.

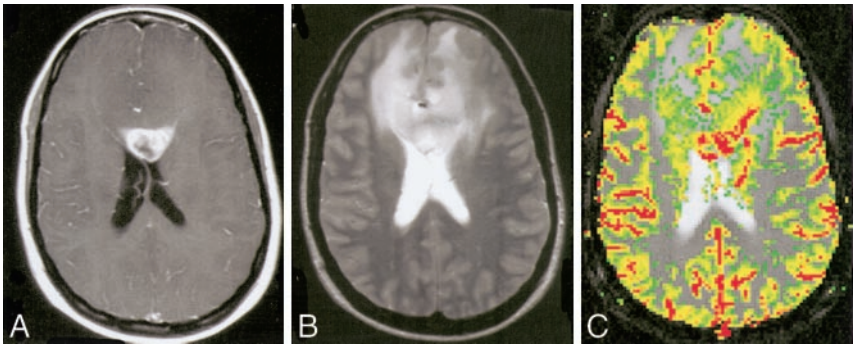

FIG 2. Images of a 34-year-old woman (patient 11) with biopsy-proved PNET.

A, Contrast-enhanced axial view T1-weighted image (600/14/1) shows a peripherally enhancing mass in the genu of the corpus callosum. Approximately 50% of the lesion enhanced. Cystic/necrotic components can be seen in the lesion.

B, Axial view T2-weighted image (3400/119/1) shows some areas of hypointensity within the mass, indicating the increased cellularity of these tumors, with a significant amount of peritumoral edema and mass effect. The signal intensity characteristics and involvement of the corpus callosum would raise the possibility of lymphoma as a differential diagnosis.

C, Gradient-echo axial view perfusion MR image (1000/54) and rCBV color overlay map show increased perfusion with a high rCBV of 6.82 and vascular permeability (K^{trans}) of 0.00034 s^{-1}. Lymphoma would appear as reduced perfusion.

Results

Conventional Imaging Findings

Ten tumors were supratentorial, and two were both supratentorial and infratentorial. Of the 10 supratentorial tumors, five were located in the frontal, two in the temporoparietal, one in the temporal, one in the suprasellar, and one the pineal region. The conventional imaging findings are summarized in Table 1. Tumor size was variable, ranging from 0.52 to 113.0 cm^3. All larger lesions were revealed to have substantial cystic and/or necrotic components (Figs 1 and 2). All tumors were iso- or hypointense on unenhanced T1-weighted images. All 12 lesions were contrast enhancing, and 10 showed enhancement of 50% or more of the lesion. The solid portion of the tumor enhanced in all cases. On T2-weighted images, the solid portions of the tumors were similar in signal intensity characteristics to gray matter; eight tumors were mainly iso- to slightly hypointense, whereas four tumors were slightly hyperintense. Moderate edema was seen in three patients, and extensive edema was present in only one (patient 11). Nine patients had cystic or necrotic components. Most tumors were well defined (n = 10) and heterogeneous in appearance (n = 10). Circumscribed susceptibility artifacts on T2-weighted images were present in three patients, indicating calcification or hemorrhage.

TABLE 3: Comparison of relative cerebral blood volume and vascular permeability measurements in patients with primitive neuroectodermal tumors with low grade gliomas (grade II/IV) and high grade gliomas (grade III/IV and IV/V)

Tumor Type	rCBV	SD	K^{trans}	SD
PNET (n = 12)	4.76	1.99	0.0033	0.0035
Low grade glioma (n = 30)	2.14	1.67	0.0005	0.001
P value	<.0005		<.05	
High grade glioma (n = 55)	5.82	3.57	0.0016	0.003
P value	0.53		0.19	

Note.—rCBV indicates relative cerebral blood volume; K^{trans}, vascular permeability (s^{-1}); PNET, primitive neuroectodermal tumor.

Perfusion Imaging Findings

rCBV measurements and vascular permeability measurements for patients with PNETs are summarized in Table 2. A comparison of rCBV and K^{trans} between PNETs and low and high grade gliomas are presented in Table 3. No statistically significant differences were found with respect to rCBV or K^{trans} when compared with a group of patients with high grade gliomas (n = 55) (mean rCBV, 5.82 ± 3.57; $P = .53$) (Fig 3) (mean K^{trans}, 0.0016 ± 0.003; $P = .19$) (Table 3). However, a statistically significant difference was noted in both rCBV and K^{trans} when compared with a group of low grade gliomas (n = 30) (mean maximum rCBV, 2.14 ± 1.67; $P < .0005$) (Fig 3) (mean maximum K^{trans}, 0.0005 ± 0.001; $P < .05$) (Table 3).

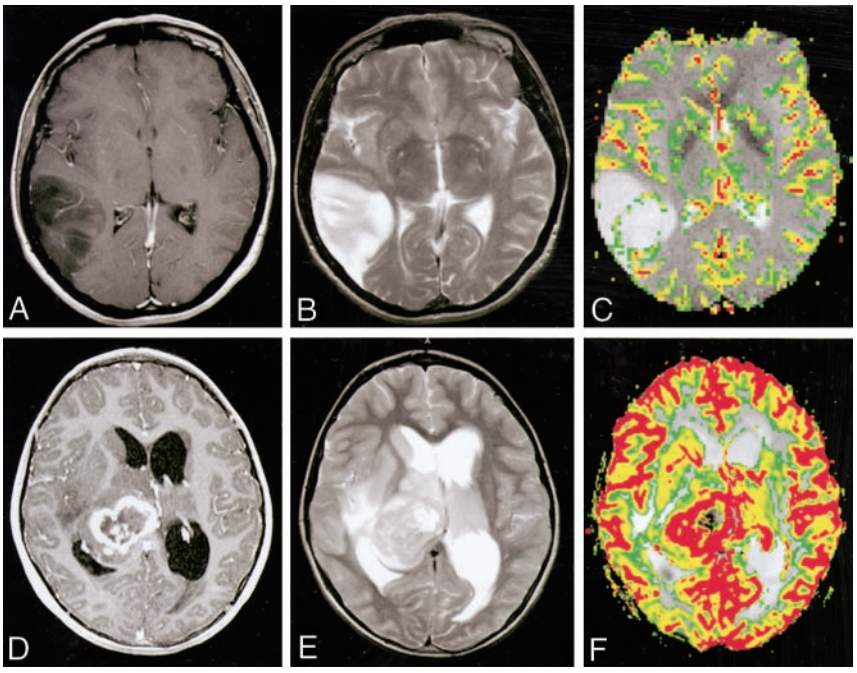

FIG 3. Images of a 52-year-old woman with a histologically confirmed grade II/IV glioma (*A*–*C*) and a 70-year-old woman with a histologically confirmed grade III/IV glioma (*D*–*F*).

A, Contrast-enhanced axial view T1-weighted image shows a lesion in the right temporoparietal region with low signal intensity and minimal enhancement.

B, Axial view T2-weighted image shows increase in T2 signal intensity within the lesion, with minimal edema.

C, Gradient-echo axial view perfusion MR image and rCBV color overlay map show a low rCBV of 1.70, in keeping with a low grade glioma. A thin rim of minimally increased perfusion can be seen at the margin of the lesion. This is compared with the increased rCBV of PNETs shown in Figures 1C and 2C.

D, Contrast-enhanced axial view T1-weighted image shows a lesion in the right thalamic region with heterogeneous peripheral contrast enhancement and a central cystic/necrotic region.

E, Axial view T2-weighted image shows increase in T2 signal intensity within the lesion with moderate surrounding edema. The patient also has hydrocephalus and transependymal edema around the ventricles.

F, Gradient-echo axial view perfusion MR image and rCBV color overlay map show a high rCBV of 3.70, in keeping with a high grade glioma. A thick rind of marked increased perfusion cannot be readily differentiated from the increased rCBV of PNETs shown in Figures 1C and 2C.

Discussion

Five-year overall survival rates are 86.3% for posterior fossa PNETs and 46.9% for patients with supratentorial PNETs (29). This seems to be related to location of the primary tumor, mitosis-karyorrhexis index, degree of differentiation, delayed diagnosis or misdiagnosis, and metastases status (29, 30). Survival statistics and knowledge regarding supratentorial and adult PNETs is limited. Hence, any information that can increase the diagnostic accuracy that may improve the survival and recurrence rates associated with these tumors would be beneficial. The most optimal treatment for PNET remains controversial (29, 31). The treatment traditionally has included surgical resection/debulking and craniospinal radiation, with or without chemotherapy (29). In the past, adjuvant radiation therapy with a craniospinal dose of 35 to 36 Gy was the criterion standard for treatment of PNETs. Recently, a new "standard" is emerging consisting of "standard dose" radiation therapy with "reduced dose" neuro-axis irradiation and then adjuvant chemotherapy with vincristine, lomustine, and cisplatin (31). Hence, supplementary pathologic or radiologic information, such as the mitosis-karyorrhexis index, degree of differentiation, metastases status, and degree of tumor perfusion, may assist in the planning of surgery, including determination of the extent of resectable tumor, dose and field of craniospinal radiation, and amount and type of chemotherapy.

PNETs are macroscopically well delineated and are more expansive than infiltrative. Cyst formation, calcifications, hemorrhage, and necrosis all can be encountered. Their cut surfaces are finely granular, pink-gray, and mostly soft in consistency. The tumors are composed of undifferentiated, densely packed neuroepithelial cells with round to oval, small, deeply basophilic nuclei and only scant surrounding cytoplasm (Fig 4). Nucleoli are not commonly seen; mitotic figures and apoptotic bodies are always present, but their extent varies greatly. The cells grow in compact sheets and form characteristic Homer-Wright rosettes (filled by neurophil) or, less frequently, Flexner-Wintersteiner rosettes (with a true central lumen). Microscopic foci of necrosis also can be seen. Although inconspicuous, a very fine fibrillar background exists due to the extensive neuronal differentiation (32). Focally, PNETs can have regions differentiated into glial, muscular, mesenchymal, or epithelial cells. Vascular endothelial hyperplasia is well described in the literature (1, 3, 33–35). PNETs usually have high proliferation rates consistent with their highly malignant potential. They can invade focally and commonly disseminate throughout the neuraxis via CSF (23). Immunohistochemistry is routinely used to identify their divergent differentiation.

Radiologic findings of PNETs have been described by several investigators (6, 36, 37). On CT scans and conventional MR images, PNETs tend to be heterogeneous masses with cystic and necrotic components, which often show contrast enhancement and may have calcification and hemorrhage. Cerebral PNETs usually are located in the temporal and temporoparietal regions, showing iso- or hypointensity on T1-weighted and iso- or hyperintensity on T2-weighted images (7). These findings are somewhat nonspecific and do not allow differentiation from other more

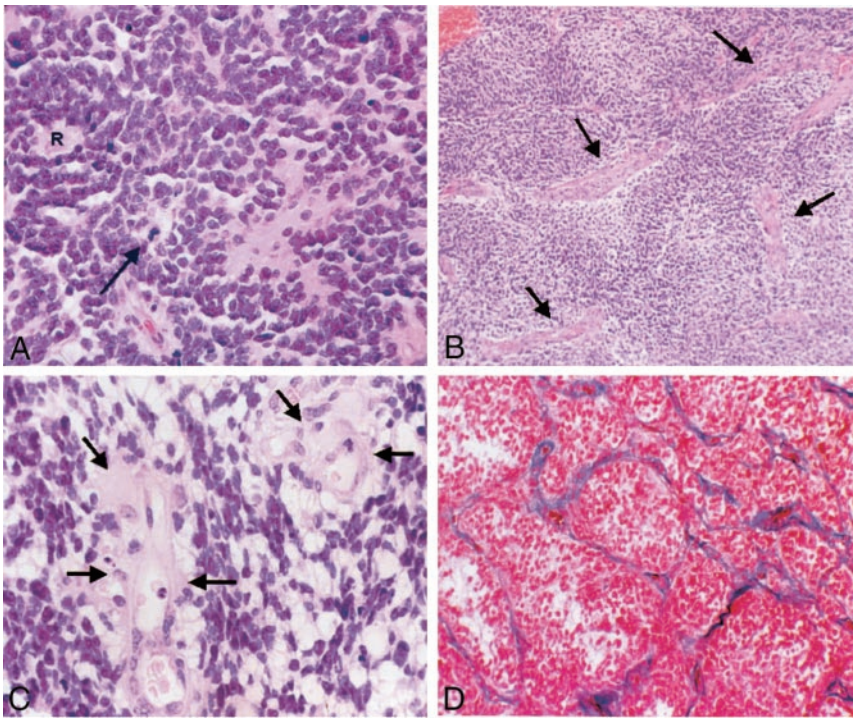

FIG 4. Photomicrographs of PNETs.

A, Hematoxylin and eosin stain shows a hypercellular neoplasm. Poorly differentiated, primitive small cells growing in compact sheets, forming a characteristic Homer-Wright rosette (*R*), can be seen. Tumor cells have round to oval hyperchromatic nuclei with scant cytoplasm. Mitotic figures are also identified (*arrow*). The increased cellularity explains iso- or hypointensity of many of the lesions on T2-weighted images (original magnification, ×200).

B, Hematoxylin and eosin stain shows increased vascular channels (*arrows*) in PNET (original magnification, ×50).

C, Hematoxylin and eosin stain at higher power shows endothelial hyperplasia (*arrows*) (original magnification, ×400).

D, Azocarmine stain highlights the vascular channels and shows proliferation and thickening of the vascular endothelium within the PNET (original magnification, ×100).

common CNS mass lesions, such as gliomas, lymphomas, and tumefactive demyelinating lesions. For example, signal intensity heterogeneity, contrast enhancement, and necrosis are found in PNETs and in high grade gliomas. The relative high cellularity and resultant iso- to hypointensity on T2-weighted images sometimes makes lymphoma a differential diagnosis.

Several series on the MR imaging findings of PNETs (6, 36–38) have reported them to be well demarcated, heterogeneous masses that nearly always contain areas of cyst or necrosis. The largest series (18 patients) (36) showed most tumors to be isointense relative to gray matter on T2-weighted and fluid-attenuated inversion recovery sequences and to be contrast enhancing on T1-weighted sequences. Calcification and hemorrhage were common findings corresponding to the pathologic features. Edema, however, is generally minimal or absent. The conventional MR imaging findings in our series seem to be consistent with those previously described in both pediatric and adult patient populations (5). On the whole, these are contrast-enhancing masses that are lobulated but well circumscribed (Table 1). Of interest is that most of the lesions (n = 8) were either iso- or hypointense on T2-weighted images, which may reflect the increased cellularity of these tumors. Conventional MR imaging findings tend to be nonspecific, with many intracranial mass lesions showing similar features (10, 39). Hence, investigators have attempted to characterize these lesions with advanced MR imaging techniques such as diffusion, perfusion, and MR spectroscopy.

Erdem et al (36) used diffusion-weighted imaging to further characterize PNETs. All their patients who underwent diffusion-weighted imaging (seven patients) had restricted diffusion. The authors theorized that this may have been related to the increased cellularity of PNETs and to their high nuclear-cytoplasm ratio, which again correlates with the relative iso- or hypointensity on T2-weighted images (Table 1, Figs 1–3). Recently, Majos et al (7) used proton MR spectroscopic imaging to study nine PNETs and found choline and lipids to be elevated compared with levels in low grade gliomas, again correlating with their highly cellular nature.

DSC MR imaging provides information regarding tumor vascularity, and elevated rCBV values have been shown to correspond to areas of microvascular density and vascular endothelial hyperplasia (40). In addition, rCBV values have been shown to correlate with tumor grade among gliomas (9–14). Vascular permeability data obtained from MR perfusion imaging may reflect the degree of blood brain–barrier disruption. Leakage across the blood brain–barrier may be due to a combination of factors, including angiogenesis and the presence of permeability factors, such as vascular endothelial growth factor (also known as vascular permeability factor) (15). Among a heterogeneous group of tumors, Roberts et al (41) found that permeability values also correlated with tumor grade. Our series found permeability values of PNETs to be similar to those of high grade gliomas.

Although increased rCBV and increased permeability seem to correlate with tumor aggressiveness, our series did not show a simple correlation between these two parameters. For example, of the five patients with rCBV values above the mean (patients 1, 5, 7, 8, and 11), only two (patients 7 and 8) had K^{trans} values above the mean. A complex relationship seems to exist between rCBV and vascular permeability. It may be possible to have increases in vascular volume without increases in vascular permeability, increases

in permeability without increases in volume, and increases in both, to varying degrees. Theoretically, factors that are involved in tumor angiogenesis should lead to both vascular hyperplasia and blood brain–barrier leakage (41). This is usually true of high grade neoplasms, which typically are shown to have elevated rCBV and permeability values. However, in this series of PNETs, they do not seem to occur to the same degree simultaneously. In a study of human breast cancer, Ryland et al (42) also showed that the tumor regions with high blood volume do not necessarily contain the vessels with the highest permeability, and vice versa. Another recent study also found that perfusion ($r = 0.62$; $P = .05$) correlated with microvessel density, but permeability moderately correlated with maximal enhancement and not with perfusion and microvessel density (18).

Our findings suggest that PNETs, which show greater contrast enhancement, also have higher permeability measurements than do low grade gliomas (Table 3), as one would expect. Four of the five patients with 70% or more of enhancement show permeability levels above the mean. Our finding of increased rCBV and vascular permeability values in PNETs can in part be attributed to histopathologic findings of vascular endothelial hyperplasia, often found in other high grade neoplasms (32, 43, 44).

In our comparison of DSC MR imaging data, PNETs showed rCBV and vascular permeability measurements similar to those of high grade gliomas; hence, rCBV and vascular permeability measurements may not be useful in differentiating PNETs from high grade gliomas (Table 3). However, increased rCBV and permeability values may be helpful in differentiating PNETs from other intracranial mass lesions. Although they behave as high grade neoplasms, the conventional MR imaging findings of PNETs may sometimes be similar to those of low grade gliomas (39), especially within the brain stem. They also may have a similar MR imaging appearance to other more common intracranial mass lesions, such as CNS lymphoma, cerebral abscesses, solitary metastatic lesions, and tumefactive demyelinating lesions (45). CNS lymphoma, either primary or secondary, has been shown to have reduced rCBV (46–48). Measurements from our institution have shown lymphoma ($n = 19$) to have rCBV of 1.44 (10) and TDLs ($n = 12$) to have a rCBV of 0.88 (45). Hence, finding elevated rCBV in PNETs may help to differentiate between PNETs and other intracranial mass lesions that show low cerebral blood volumes, such as CNS lymphoma and tumefactive demyelinating lesions.

On the basis of conventional MR imaging findings alone, only two patients were assigned the preoperative diagnosis of PNET (patients 6 and 8). Four patients were considered to have high grade gliomas based on conventional MR imaging findings. Hence, the diagnosis for these six patients did not alter after the DSC MR imaging analysis. Of the remaining six patients, two were considered to possibly have low grade gliomas based on the conventional MR imaging findings, three were diagnosed as having lymphoma, and one was diagnosed as having either lymphoma or low grade glioma (patient 1). For these six patients (50% of patients), DSC MR imaging changed the final preoperative diagnosis to either high grade glioma or PNET based on the increased rCBV and K^{trans}.

Intracranial tumors are characterized by bizarre and extreme tortuosity in the morphology of the angioarchitecture. It has been shown that the blood flow through the tumor vasculature is extremely variable and heterogeneous within any given region of a tumor (49, 50). Multiple factors influence the leakiness of a blood vessel, including a luminal surface area, permeability of the vessel wall, blood flow, and hydrostatic, interstitial, and osmotic gradients across the endothelium (49, 51, 52). Hence, K^{trans} may be underestimated if extremely slow flow or low hydrostatic/osmotic gradients are present in a group of extremely tortuous vessels or in cases of substantial vasogenic edema. Although it is, in principle, possible to form maps of K^{trans} on a pixel-by-pixel basis, the calculation can be sensitive to noise and is time-consuming. We therefore calculated K^{trans} only on regions of interest. However, to present a visual indication of contrast medium leakage, we also calculated maps of the fractional signal intensity drop at 25 sesconds after the bolus (SD25 maps). The choice of 25 seconds is arbitrary but was based on our observation that the bolus had always passed and was returning to baseline by that time and that it also always fell within our 1-minute acquisition. If vascular permeability is high, residual contrast concentration also is high after the bolus has passed; hence, the SD25 value also is high. Conversely, if permeability is low, the signal intensity rapidly returns close to the unenhanced baseline and the SD25 value is low. The SD25 maps therefore provide a simple index related to vascular permeability that can be used to select regions of interest for K^{trans} calculation. K^{trans} was calculated in regions of interest showing the highest SD25 values. SD25 is not exactly correlated with vascular permeability because other factors, such as cardiac output and dose of contrast medium, will affect its value. However, within an individual case in which those factors are constant, high correlation is likely to be found (although not a linear one). We have previously found high correlations between empirical indices such as SD25 and more exact parameters (53).

Several methods are available to determine K^{trans}. The method used by Roberts et al (41) is based on measurements acquired during the washout of contrast medium from the tumor. At this time, vascular contrast medium concentration is low relative to extravascular contrast medium concentration. Consequently, cerebral blood volume measurements obtained in this way may be less accurate than those obtained on the basis of the intravascular indicator dilution theory, which are acquired during the presence of contrast medium bolus when vascular concentration is high. Conversely, measurements of K^{trans} by first pass pharmacokinetic modeling may be less accurate than those reported by Roberts et al because

first pass pharmacokinetic modeling data are acquired only during the first pass of the bolus, although this has yet to be determined. Two other differences exist between our approach and that presented by Roberts et al. The former is based on T2* changes and the latter on T1 changes. The former requires correction for leakage of contrast medium, whereas the latter takes this inherently into account. It is not clear, however, what effect these differences will have on vascular permeability measurements.

Using a gradient-echo echo-planar imaging sequence becomes problematic in the setting of significant necrosis or hemorrhage. Significant susceptibility from necrosis and hemorrhage may affect our measurements of rCBV and K^{trans}. However, review of the conventional MR images showed few lesions to have significant hemorrhage to adversely affect our measurements. Substantial mass effect from the tumor and vasogenic edema also may potentially reduce vascular permeability, because this may alter the hydrostatic and interstitial gradients across vascular endothelium (49, 52, 54, 55). Hence, it would be interesting to determine the relationship between the degree of vasogenic edema and mass effect on K^{trans} measurements.

Another potential limitation of this study is the relatively older age of our patient group. Our sample may not be representative of PNETs that occur in younger patients. Some investigators have suggested that there may be a delayed onset variant of PNET, as is the case with craniopharyngiomas, and that there may be two peaks in the age profile for PNET, a younger pediatric age group and an older middle age peak (5). The relatively large number (n = 12) of this rare tumor in this single institutional analysis also is explained by the substantial referral of adult brain tumors to our institution during a 7-year period. Another recent analysis conducted at a single institution for a 10-year period also presented 12 adult patients with supratentorial PNETs (5).

For neurosurgeons, any and all preoperative information regarding the nature of a tumor affects surgical decision making before and during surgery. Supplemental information regarding the aggressive nature of a tumor may alter the risk-benefit analysis conducted by the neurosurgeon. Identifying PNETs preoperatively in adults is greatly advantageous for neurosurgeons, especially considering that the differential diagnosis of these lesions often includes low grade glioma or lymphoma. CNS lymphoma generally is not a surgical entity; only biopsy is required because the treatment usually is high dose chemotherapy and/or irradiation. Treatment of most adult PNETs benefits from aggressive surgical resection to attain limited residual or no residual disease before adjuvant therapy (29). Practically speaking, the neurosurgeon confronted with a contrast-enhancing, highly cellular tumor shown by preoperative MR imaging will often rely on intraoperative frozen section diagnosis to decide between limited biopsy and aggressive resection. Alternatively, some surgeons will opt for a two-stage process of stereotactic biopsy and then craniotomy. Preoperative suspicion of PNET based on DSC MR imaging allows the neurosurgeon to proceed aggressively. More importantly, it bolsters the surgeon's faith in the intraoperative pathologic diagnosis of PNET. Few surgeons would like to discover that they have performed aggressive resection and then be informed that the final pathologic findings show lymphoma. The analysis holds true for preoperative identification of low grade gliomas in or near eloquent areas of the brain. Again, the neurosurgeon may elect preoperatively or intraoperatively to limit his or her resection to preserve function when dealing with suspected low grade lesions.

Finally, the preoperative estimation of the vascularity of a lesion is always of use to the surgeon. Being armed and ready to fight a vascular tumor is always preferable to an unpleasant intraoperative surprise. After surgery, the vascularity of a lesion may enter into the decision to provide aggressive adjuvant therapy. Although the pathologic findings may be interpreted as a PNET, increased rCBV, considered along with proliferation indices, may be one of the characteristics of a lesion that induces the treating team to proceed with adjuvant therapy. It may well affect the choice of adjuvant therapies, especially the use of anti-angiogenesis strategies.

Conclusion

The conventional MR imaging findings in adult PNETs can be variable and nonspecific. rCBV and vascular permeability measurements in PNETs are elevated and have histopathologic correlates such as endothelial hyperplasia and blood brain–barrier disruption. No statistically significant difference in rCBV and K^{trans} was observed between adult PNETs and high grade gliomas. However, perfusion MR imaging may be useful in differentiating PNETs from other intracranial mass lesions with similar conventional MR imaging findings but relatively lower perfusion parameters, such as low grade gliomas, tumefactive demyelinating lesions, and lymphomas. Furthermore, for neurosurgeons, any and all preoperative information on the nature of a tumor affects surgical decision making before and during surgery.

References

1. Gaffney CC, Sloane JP, Bradley NJ, Bloom HJ. **Primitive neuroectodermal tumors of the cerebrum: pathology and treatment**. *J Neurooncol* 1985;3:23–33
2. Masuda K, Yutani C, Akutagawa K, et al. **Cerebral primitive neuroectodermal tumor in an adult male: a case report**. *Acta Cytol* 2000;44:1050–1058
3. Bellis EH, Salcman M, Bastian FO. **Primitive neuroectodermal tumor in a 57-year-old man**. *Surg Neurol* 1983;20:30–35
4. Grant G, Pathak S, Maria BL. **Identification of marker chromosomes in a human medulloblastoma cell line (D283 Med)**. *Cancer Genet Cytogenet* 1988;34:247–250
5. Kim DG, Lee DY, Paek SH, Chi JG, Choe G, Jung HW. **Supratentorial primitive neuroectodermal tumors in adults**. *J Neurooncol* 2002;60:43–52
6. Pickuth D, Leutloff U. **Computed tomography and magnetic resonance imaging findings in primitive neuroectodermal tumors in adults**. *Br J Radiol* 1996;69:1–5

7. Majos C, Alonso J, Aguilera C, et al. **Adult primitive neuroectodermal tumor: proton MR spectroscopic findings with possible application for differential diagnosis**. *Radiology* 2002;225:556–566
8. Brandes AA, Palmisano V, Monfardini S. **Medulloblastoma in adults: clinical characteristics and treatment**. *Cancer Treat Rev* 1999;25:3–12
9. Aronen HJ, Gazit IE, Louis DN, et al. **Cerebral blood volume maps of gliomas: comparison with tumor grade and histologic findings**. *Radiology* 1994;191:41–51
10. Cha S, Knopp EA, Johnson G, Wetzel SG, Litt AW, Zagzag D. **Intracranial mass lesions: dynamic contrast-enhanced susceptibility-weighted echo-planar perfusion MR imaging**. *Radiology* 2002; 223:11–29
11. Knopp EA, Cha S, Johnson G, et al. **Glial neoplasms: dynamic contrast-enhanced T2*-weighted MR imaging**. *Radiology* 1999;211: 791–798
12. Lev MH, Rosen BR. **Clinical applications of intracranial perfusion MR imaging**. *Neuroimaging Clin N Am* 1999;9:309–331
13. Shin JH, Lee HK, Kwun BD, et al. **Using relative cerebral blood flow and volume to evaluate the histopathologic grade of cerebral gliomas: preliminary results**. *AJR Am J Roentgenol* 2002;179:783–789
14. Sugahara T, Korogi Y, Kochi M, et al. **Correlation of MR imaging-determined cerebral blood volume maps with histologic and angiographic determination of vascularity of gliomas**. *AJR Am J Roentgenol* 1998;171:1479–1486
15. Provenzale JM, Wang GR, Brenner T, Petrella JR, Sorensen AG. **Comparison of permeability in high-grade and low-grade brain tumors using dynamic susceptibility contrast MR imaging**. *AJR Am J Roentgenol* 2002;178:711–716
16. Roberts HC, Roberts TP, Ley S, Dillon WP, Brasch RC. **Quantitative estimation of microvascular permeability in human brain tumors: correlation of dynamic Gd-DTPA-enhanced MR imaging with histopathologic grading**. *Acad Radiol* 2002;9[suppl 1]:S151–S155
17. Uematsu H, Maeda M, Sadato N, et al. **Vascular permeability: quantitative measurement with double-echo dynamic MR imaging: theory and clinical application**. *Radiology* 2000;214:912–917
18. Kiessling F, Krix M, Heilmann M, et al. **Comparing dynamic parameters of tumor vascularization in nude mice revealed by magnetic resonance imaging and contrast-enhanced intermittent power Doppler sonography.** *Invest Radiol* 2003;38:516–524
19. Bogin L, Margalit R, Mispelter J, Degani H. **Parametric imaging of tumor perfusion using flow- and permeability-limited tracers**. *J Magn Reson Imaging* 2002;16:289–299
20. Marzola P, Farace P, Calderan L, et al. **In vivo mapping of fractional plasma volume (fpv) and endothelial transfer coefficient (Kps) in solid tumors using a macromolecular contrast agent: correlation with histology and ultrastructure.** *Int J Cancer* 2003; 104:462–468
21. Christoforidis GA, Grecula JC, Newton HB, et al. **Visualization of microvascularity in glioblastoma multiforme with 8-T high-spatial-resolution MR imaging**. *AJNR Am J Neuroradiol* 2002;23:1553–1556
22. Christoforidis GA, Bourekas EC, Baujan M, et al. **High resolution MRI of the deep brain vascular anatomy at 8 Tesla: susceptibility-based enhancement of the venous structures.** *J Comput Assist Tomogr* 1999;23:857–866
23. Kleihues P, Soylemezoglu F, Schauble B, Scheithauer BW, Burger PC. **Histopathology, classification, and grading of gliomas**. *Glia* 1995;15:211–221
24. Rosen BR, Belliveau JW, Vevea JM, Brady TJ. **Perfusion imaging with NMR contrast agents**. *Magn Reson Med* 1990;14:249–265
25. Wetzel SG, Cha S, Johnson G, et al. **Relative cerebral blood volume measurements in intracranial mass lesions: interobserver and intraobserver reproducibility study**. *Radiology* 2002;224:797–803
26. Johnson G, Wetzel S, Cha S, Babb J, Tofts PS. **Measuring blood volume and vascular transfer constant by dynamic T2*-weighted contrast-enhanced MRI**. *Magn Reson Med* 2004;51. In press
27. Tofts PS, Kermode AG. **Measurement of the blood-brain barrier permeability and leakage space using dynamic MR imaging: fundamental concepts.** *Magn Reson Med* 1991;17:357–367
28. Tofts PS, Brix G, Buckley DL, et al. **Estimating kinetic parameters from dynamic contrast-enhanced T(1)-weighted MRI of a diffusable tracer: standardized quantities and symbols**. *J Magn Reson Imaging* 1999;10:223–232
29. Paulino AC, Melian E. **Medulloblastoma and supratentorial primitive neuroectodermal tumors: an institutional experience**. *Cancer* 1999;86:142–148
30. Shimada H, Umehara S, Monobe Y, et al. **International neuroblastoma pathology classification for prognostic evaluation of patients with peripheral neuroblastic tumors**. *Cancer* 2001;92:2451–2461
31. Saran F. **Recent advances in pediatric neuro-oncology**. *Curr Opin Neurol* 2002;15:671–677
32. Burger PC, Vogel FS. **The brain: tumors.** In: Burger PC, Vogel FS, eds. *Surgical Pathology of the Central Nervous System and Its Coverings.* New York: Wiley;1982:223–266
33. Hart MN, Earle KM. **Primitive neuroectodermal tumors of the brain in children**. *Cancer* 1973;32:890–897
34. Kosnik EJ, Boesel CP, Bay J, Sayers MP. **Primitive neuroectodermal tumors of the central nervous system in children**. *J Neurosurg* 1978;48:741–746
35. Duffner PK, Cohen ME, Heffner RR, Freeman AI. **Primitive neuroectodermal tumors of childhood: an approach to therapy**. *J Neurosurg* 1981;55:376–381
36. Erdem E, Zimmerman RA, Haselgrove JC, Bilaniuk LT, Hunter JV. **Diffusion-weighted imaging and fluid attenuated inversion recovery imaging in the evaluation of primitive neuroectodermal tumors**. *Neuroradiology* 2001;43:927–933
37. Figeroa RE, el Gammal T, Brooks BS, Holgate R, Miller W. **MR findings on primitive neuroectodermal tumors**. *J Comput Assist Tomogr* 1989;13:773–778
38. Zagzag D, Miller DC, Knopp EA, et al. **Primitive neuroectodermal tumors of the brainstem: investigation of seven cases**. *Pediatrics* 2000;106:1045–1053
39. Osborn AG. *Diagnostic Neuroradiology.* St. Louis: Mosby; 1994
40. Cha S, Johnson G, Wadghiri YZ, et al. **Dynamic, contrast-enhanced perfusion MRI in mouse gliomas: correlation with histopathology.** *Magn Reson Med* 2003;49:848–855
41. Roberts HC, Roberts TPL, Brasch RC, Dillon WP. **Quantitative measurement of microvascular permeability in human brain tumors achieved using dynamic contrast-enhanced MR imaging: correlation with histologic grade**. *AJNR Am J Neuroradiol* 2000;21: 891–899
42. Rydland J, BjOrnerud A, Haugen O, et al. **New intravascular contrast agent applied to dynamic contrast enhanced MR imaging of human breast cancer**. *Acta Radiol* 2003;44:275–283
43. Brem S. **Angiogenesis and cancer control: from concept to therapeutic trial**. *Cancer Control* 1999;6:436–458
44. Daumas-Duport C, Scheithauer B, O'Fallon J, Kelly P. **Grading of astrocytomas: a simple and reproducible method**. *Cancer* 1988;62: 2152–2165
45. Cha S, Pierce S, Knopp EA, et al. **Dynamic contrast-enhanced T2*-weighted MR imaging of tumefactive demyelinating lesions**. *AJNR Am J Neuroradiol* 2001;22:1109–1116
46. Hartmann M, Heiland S, Harting I, et al. **Distinguishing of primary cerebral lymphoma from high-grade glioma with perfusion-weighted magnetic resonance imaging**. *Neurosci Lett* 2003;338:119–122
47. Law M, Teicher N, Zagzag D, Knopp EA. **Dynamic contrast enhanced perfusion MRI in mycosis fungoides**. *J Magn Reson Imaging* 2003;18:364–367
48. Sugahara T, Korogi Y, Shigematsu Y, et al. **Perfusion-sensitive MRI of cerebral lymphomas: a preliminary report**. *J Comput Assist Tomogr* 1999;23:232–237
49. McDonald DM, Choyke PL. **Imaging of angiogenesis: from microscope to clinic**. *Nat Med* 2003;9:713–725
50. Vajkoczy P, Menger MD. **Vascular microenvironment in gliomas**. *J Neurooncol* 2000;50:99–108
51. Li KL, Zhu XP, Checkley DR, et al. **Simultaneous mapping of blood volume and endothelial permeability surface area product in gliomas using iteractive analysis of first-pass dynamic contrast enhanced MRI data**. *Br J Radiol* 2003;76:39–51
52. McDonald DM, Baluk P. **Significance of blood vessel leakiness in cancer**. *Cancer Res* 2002;62:5381–5385
53. Cha S, Lu S, Johnson G, Knopp EA. **Dynamic susceptibility contrast MR imaging: correlation of signal intensity changes with cerebral blood volume measurements**. *J Magn Reson Imaging* 2000; 11:114–119
54. Bhujwalla ZM, Artemov D, Natarajan K, Solaiyappan M, Kollars P, Kristjansen PE. **Reduction of vascular and permeable regions in solid tumors detected by macromolecular contrast magnetic resonance imaging after treatment with antiangiogenic agent TNP-470**. *Clin Cancer Res* 2003;9:355–362
55. Degani H, Chetrit-Dadiani M, Bogin L, Furman-Haran E. **Magnetic resonance imaging of tumor vasculature**. *Thromb Haemost* 2003;89:23–33